Is stomatal conductance optimised over both time and space in plant crowns? A field test in grapevine (*Vitis vinifera*).

Thomas N Buckley [†,1,*]
Sebastia Martorell [†,2]
Antonio Diaz-Espejo [3]
Magdalena Tomàs [2]
Hipólito Medrano [2]

[1] IA Watson Grains Research Centre, Faculty of Agriculture and Environment, The University of Sydney, Narrabri, NSW Australia.
[2] Research Group on Plant Biology under Mediterranean Conditions, Departament de Biologia, Universitat de les Illes Balears, Carretera de Valldemossa Km 7.5, 07122 Palma de Mallorca, Illes Balears, Spain.
[3] Irrigation and Crop Ecophysiology Group, Instituto de Recursos Naturales y Agrobiología de Sevilla (IRNAS, CSIC). Avenida Reina Mercedes 10, 41012 Sevilla, Spain.

*Corresponding author:
t.buckley@sydney.edu.au
+61 0481 009 451

[†] These authors contributed equally to the authorship of this work

Abstract

Crown carbon gain is maximised for a given total water loss if stomatal conductance (g_s) varies such that the marginal carbon product of water ($\partial A/\partial E$) remains invariant both over time and among leaves in a plant crown, provided the curvature of assimilation rate (A) vs transpiration rate (E) is negative. We tested this prediction across distinct crown positions *in situ* for the first time, by parameterising a biophysical model across 14 positions in four grapevine crowns (*Vitis vinifera*), computing optimal patterns of g_s and E over a day and comparing these to observed patterns. Observed water use was higher than optimal for leaves in the crown interior, but lower than optimal in most other positions. Crown carbon gain was 18% lower under measured g_s than under optimal g_s. Positive curvature occured in 39.6% of cases due to low boundary layer conductance (g_{bw}), and optimal g_s was zero in 11% of cases because $\partial A/\partial E$ was below the target value at all g_s. Some conclusions changed if we assumed infinite g_{bw}, but optimal and measured E still diverged systematically in time and space. We conclude that the theory's spatial dimension and assumption of positive curvature require further experimental testing.

Keywords: optimisation, stomata, boundary layer, water use efficiency, carbon water balance.

Introduction

Water is a major factor limiting plant growth and carbon sequestration in both natural and agricultural systems. To predict and manage these systems and to direct basic research into the underlying biological controls, we need formal mathematical models that can both predict and explain how carbon and water exchange are coordinated and regulated by stomatal conductance (g_s). However, no process-based model of g_s that can achieve this has yet gained consensus, and phenomenological models merely reproduce observed patterns of g_s, so they have limited ability to explain stomatal behaviour (Damour *et al.*, 2010, Buckley & Mott, 2013). Another approach, optimisation theory, attempts to deduce g_s from the hypothesis that stomatal behaviour tends to maximise carbon gain (net CO_2 assimilation rate, A) for a given water loss (transpiration rate, E) (Cowan & Farquhar, 1977). The rationale for this hypothesis is that natural selection has presumably favoured genotypes with more nearly optimal use of limiting resources, including water (Cowan & Farquhar, 1977, Cowan, 2002, Mäkelä *et al.*, 2002).

Formally, the optimisation hypothesis states that, among all possible spatio-temporal distributions of g_s that yield the same total transpiration rate, total carbon gain will be greatest for the distribution in which the ratio of the marginal sensitivities of A and E to g_s ($(\partial A/\partial g_s)/(\partial E/\partial g_s)$, often abbreviated as $\partial A/\partial E$ and referred to in this study as the *marginal carbon product of water*) is invariant within the domain in which total transpiration rate can be considered constant (Cowan & Farquhar, 1977). That domain is typically taken to be one day (at longer time scales, the total water supply available to the canopy, and with it the target value μ for $\partial A/\partial E$, may change). This result assumes that the A vs E curve generated by varying g_s has negative curvature; i.e., $\partial A/\partial E$ always declines when E increases by stomatal opening ($\partial^2 A/\partial E^2 < 0$).

Pioneering work by Farquhar (1973) and Cowan and Farquhar (1977) showed that the patterns of stomatal behaviour predicted by this hypothesis share important qualitative features with observed behaviour, including reduced g_s under high evaporative demand or low light (photosynthetic photon flux density, PPFD).

The subsequent four decades have seen this theory tested many times – most commonly in relation to controlled variations in individual environmental variables such as evaporative demand, but also in relation to natural variation in environmental conditions *in situ* (e.g., Farquhar *et al.*, 1980a, Meinzer, 1982, Williams, 1983, Ball & Farquhar, 1984, Küppers, 1984, Sandford & Jarvis, 1986, Guehl & Aussenac, 1987, Fites & Teskey, 1988, Berninger *et al.*, 1996, Hari *et al.*, 1999, Thomas *et al.*, 1999, Schymanski *et al.*, 2008, Way *et al.*, 2011). However, two critical elements of the original theory remain largely untested: neither its spatial dimension – that is, the prediction that $\partial A/\partial E$ should not vary among leaves at distinct crown positions within the same individual – nor the assumption that $\partial^2 A/\partial E^2 < 0$ have ever been tested in the field. The prediction that the target value of $\partial A/\partial E$ should be the same for all leaves in the canopy follows from the premise that the plant has a single total water supply, and the ability, in principle, to distribute water arbitrarily among leaves. The original Cowan-Farquhar theory does not distinguish temporal and spatial variations in $\partial A/\partial E$, either of which will reduce whole-canopy carbon gain (provided $\partial^2 A/\partial E^2 < 0$). Furthermore, few tests have accounted for variations in mesophyll and boundary layer conductances (g_m and g_{bc}, respectively), both of which restrict CO_2 diffusion and can strongly influence the predictions and assumptions of optimisation theory (Buckley *et al.*, 1999, Buckley *et al.*, 2013, Buckley & Warren, 2013).

The objective of this study was to test the spatial dimension of the optimisation hypothesis and its assumption of negative curvature in A vs E, while accounting for mesophyll and boundary layer conductances. We parameterised a biochemical gas exchange model (which included mesophyll conductance and its temperature response) for one leaf at each of 14 standardised positions in each of four individual crowns of grapevine (*Vitis vinifera* L. var Grenache), and then monitored *in situ* environmental conditions and stomatal conductance for each of those leaves over time across a single day. We used these data to test the theory's assumption that $\partial^2 A/\partial E^2 < 0$, to infer the optimal spatio-temporal distributions of g_s (and E), and to compare the inferred optimal patterns with observed patterns.

Materials and methods

Study system

This study was conducted from 17 to 24 August 2012 in the experimental field of the University of Balearic Islands during summer 2012 on grapevines of Grenache varietal. Soil was a clay loam type 1.5 m deep. Plants were 3-years-old grafted on rootstock Richter-110 and planted in rows (distance between rows was 2.5 m and between plants, 1 m). Plants were situated in a bilateral double cordon having between 10-12 canes per plant. Plants had been irrigated throughout the summer with 9.0 liters per plant per day, an amount that had been established as adequate to sustain high plant water status in a previous experiment. Predawn water potential of plants on the day of *in situ* gas exchange measurements (22 August 12) was -0.24 ± 0.06 MPa.

Four plants and 14 crown positions of each plant were selected for gas exchange measurements. Four of these positions were on the east face of the crown (positions 1-4), two were on the top of

the crown (5 & 6), four were on the west face (7-10), and four were located in the inner part of the crown (11-14). These crown positions are illustrated in Figure 1.

Meteorological measurements

A meteorological station (Meteodata-3000) located in the experimental field with sensors of wind speed (Young 81000, R.M. Young company, Traverse City, Michigan) and air temperature and relative humidity (Young 41382, Young company) were used. The height of the wind speed sensor was 2.7 meters above the soil (approximately 0.5 meters above the upper part of the canopy).

Biophysical gas exchange model

We used the photosynthesis model of Farquhar et al (1980b) and the gas-exchange equations of von Caemmerer and Farquhar (1981) to simulate CO_2 and H_2O exchange in grapevine. Briefly, the net CO_2 assimilation rate due to biochemical demand (A_d) is computed from RuBP-carboxylation-limited and –regeneration-limited rates (A_v and A_j) (a list of symbols is given in Table 1):

(1) $$A_v = V_m \frac{c_c - \Gamma_*}{c_c + K_c\left(1 + O/K_o\right)} - R_d$$, and

(2) $$A_j = \tfrac{1}{4} J \frac{c_c - \Gamma_*}{c_c + 2\Gamma_*} - R_d$$,

where V_m is carboxylation capacity, J is potential electron transport rate, c_c is chloroplastic CO_2 concentration, Γ_* is photorespiratory CO_2 compensation point, K_c and K_o are the Michaelis

137 constants for RuBP carboxylation and oxygenation, respectively, O is oxygen concentration and
138 R_d is the rate of non-photorespiratory CO_2 release. Actual assimilation rate is calculated as the
139 hyperbolic minimum of A_v and A_j (the lesser root A_d of $\theta_A A_d^2 - A_d(A_v + A_j) + A_v A_j = 0$, where θ_A is
140 a dimensionless curvature parameter less than unity); this accounts for co-limitation by both
141 carboxylation and regeneration near the transition between the two limitations, and it smoothes
142 the transition, ensuring differentiability as required for continuous optimisation. We calculated J
143 as the hyperbolic minimum of light-limited and light-saturated rates, J_m and J_i (the lesser root J
144 of $\theta_J J^2 - J(J_m + J_i) + J_m J_i = 0$; $J_i = 0.5\alpha \cdot (1 - f) \cdot \mathrm{PPFD}$, α is the leaf absorptance to photosynthetic
145 irradiance and f is the fraction of absorbed photons that do not contribute to photochemistry).
146
147 The supply of CO_2 by diffusion to the sites of carboxylation (A_s) was modeled as
148
149 (3) $$A_s = g_{tc}(c_a - c_c),$$
150
151 where g_{tc} is total conductance to CO_2, given by
152
153 (4) $$g_{tc} = \left(g_{sc}^{-1} + g_{bc}^{-1} + g_m^{-1}\right)^{-1},$$
154
155 where g_{sc} is stomatal conductance to CO_2 (g_s/1.6 where g_s is stomatal conductance to H_2O), g_{bc} is
156 boundary layer conductance to CO_2 and g_m is mesophyll conductance to CO_2. At steady state,
157 the supply and demand rates are equal ($A_d = A_s$), so the actual net CO_2 assimilation rate, A, is
158 given by the intersection of A_d and A_s:
159

(5) $A = A_d \cap A_s$.

This intersection leads to a quartic (4th-order polynomial) expression for c_c, whose coefficients are functions of the parameters in Eqns 1-3, and which is readily solved for c_c (e.g., Abramowitz & Stegun, 1972). Transpiration rate (E) is given by

(6) $E = g_{tw}\Delta w$,

where

(7) $g_{tw} = \left(g_s^{-1} + g_{bw}^{-1}\right)^{-1}$, and

(8) $\Delta w = \frac{w_i - w_a}{1 - \frac{1}{2}\cdot 0.001\cdot\left(w_i + w_a\right)}$,

in which g_{bw} is boundary layer conductance to H_2O and w_i and w_a are the water vapour mole fractions in the intercellular spaces and the ambient air, respectively. We assumed that the air spaces were saturated with water vapour, so that w_i was given by

(9) $w_i = 6.112\cdot\exp\left(17.62\cdot T_{leaf}/\left(243.13 + T_{leaf}\right)\right)/P_{atm}$,

where T_{leaf} is leaf temperature in ^{o}C (World Meteorological Organization, 2008). The expression in the numerator of Eqn 9 gives the saturation partial pressure of water, and P_{atm} is total

atmospheric pressure. We estimated *in situ* leaf temperature using the isothermal net radiation approximation as described by Leuning et al. (1995) and modified to molar units:

$$T_{leaf} = T_{air} + \frac{\gamma R_n^* / c_p - D_a g_{tw}}{s g_{tw} + \gamma (g_{bh} + g_{Rn})} \quad (10)$$

where T_{air} is air temperature, γ is the psychrometric constant, c_p is the molar heat capacity of air, D_a is the saturation vapour pressure deficit of air, and s is the derivative of saturation vapour pressure with respect to temperature. g_{Rn} is the radiation conductance, given by

$$g_{Rn} = 4\varepsilon_{leaf} k_d f_{ir} \sigma T_{air}^3 / c_p , \quad (11)$$

where ε_{leaf} is leaf emissivity to longwave radiation, σ is the Stefan-Boltzmann constant, k_d is the canopy extinction coefficient for diffuse irradiance (0.8; Leuning *et al.*, 1995), and f_{ir} is the fraction of the leaf's incoming infrared radiation that comes directly from the sky. In simulations on horizontally continuous canopies, f_{ir} is generally taken as $\exp(-k_d L)$ where L is cumulative leaf area index (e.g., Leuning *et al.*, 1995). We computed f_{ir} in this fashion for interior crown leaves (positions 11-14); for positions on the lateral crown exterior (positions 1-4 and 7-10), we computed f_{ir} as the fraction of each leaf's upwards sky view occupied by actual sky rather than by the adjacent canopy ($\beta/180$, where β (degrees) is the angle at which sky appears above the adjacent canopy, as viewed from the crown position in question). We used $f_{ir} = 1.0$ for the two positions at the top of the crown (positions 5 and 6). R_n^* is the isothermal net radiation, given by

(12) $$R_n^* = \Phi - (1 - \varepsilon_{atm}) k_d f_{ir} \sigma T_{air,K}^4$$

where Φ is absorbed shortwave radiation, ε_{atm} is atmospheric emissivity to longwave radiation, given by $0.642 \cdot (0.001 \cdot P_{atm} \cdot w_a / T_{air,K})^{1/7}$ for P_{atm} in Pa and w_a in mmol mol^{-1} (Leuning *et al.*, 1995), and $T_{air,K}$ is T_{air} in Kelvins. Note that this assumes a canopy IR emissivity of unity. We calculated Φ by assuming incident shortwave radiation was equal to 0.5666·PPFD (0.5666 is the ratio of total shortwave energy to photosynthetic photon flux in extraterrestrial solar radiation; de Pury & Farquhar, 1997), and that this radiation was half visible and half near-infrared (Leuning *et al.*, 1995), with leaf absorptances of 0.92 and 0.2, respectively (0.92 was the mean observed PAR absorptance of leaves in this study, and 0.2 is the complement of NIR reflection and transmission coefficients, both of which are approximately 0.4; Gates *et al.*, 1965). This gives Φ = (0.5·0.92 + 0.5·0.2)·0.5666·PPFD = 0.3173·PPFD.

Equation 10 requires a value for boundary layer conductances to heat (g_{bh}) and water (g_{bw}, which is embedded in g_{tw} (Eqn 7)), and Eqn 4 requires boundary layer conductance to CO_2 (g_{bc}). We assumed $g_{bc} = g_{bw}/1.37$ and $g_{bw} = 1.08 \cdot g_{bh}$ and simulated g_{bh} using an expression based on forced (wind-driven) convection (Leuning *et al.*, 1995):

(13) $$g_{bh} = 0.123 \left(v_{wind} / d_{leaf} \right)^{0.5}$$

where v_{wind} is wind speed and d_{leaf} is the leaf's characteristic dimension (approximately equivalent to its average downwind width; 0.1 m in this study). This ignores the possibility of free convection driven by buoyancy of air warmed by the leaf. However, most available data

and theoretical studies suggest that free convection contributes only negligibly to heat exchange under natural conditions, even at very low wind speeds, and that modeling g_{bh} based on forced convection alone provides accurate predictions (Leuning, 1988, Brenner & Jarvis, 1995, Grantz & Vaughn, 1999, Roth-Nebelsick, 2001). We simulated the attenuation of wind speed through the canopy profile by

$$v_{wind} = v_{wind(top)} \cdot \exp(-0.5L) \quad (14)$$

where L is cumulative leaf area index (m^2 m^{-2}) and $v_{wind(top)}$ is the wind speed measured above the canopy. To calculate L for each canopy position, we summed the leaf area index of all canopy regions (as defined by Figure 1) above that position. To measure those leaf area indices, we measured the total leaf area in each canopy region for each of six individuals, then divided these areas by the projected areas of each region to give the leaf area index contributed by that region. The resulting values of L are given in Table 2.

Parameterising the gas exchange model

We estimated photosynthetic parameters for each of 56 leaves (four individuals x 14 canopy positions) as follows. We measured the response of leaf net CO_2 assimilation rate (A) to intercellular CO_2 mole fraction (c_i) using an open flow gas exchange system (Li-6400; Li-Cor, Inc., Lincoln, Nebraska) equipped with an integrated leaf chamber fluorometer (Li-6400-40; Li-Cor). Curves were performed under saturating light (1500 μmol $m^{-2}s^{-1}$), with block temperature controlled at 30ºC. Ambient CO_2 (c_a) was set between 50 and 1600 μmol mol^{-1} and chamber humidity was set to track ambient conditions. After steady state photosynthesis was reached, c_a

was lowered stepwise from 400 to 50 μmol mol^{-1}, returned to 400 μmol mol^{-1} and increased stepwise to 1600 μmol mol^{-1}. A total of 16 points were recorded for each curve. We then estimated g_m, V_m and J_m by the curve fitting method proposed by Ethier & Livingston (2004). To simulate changes in these parameters with temperature, we corrected these values to 25ºC (as g_{m25}, V_{m25} and J_{m25}, respectively) using temperature responses measured on leaves of the same variety, grown in pots at the same site and transported to the laboratory to allow plants to acclimate to constant temperature and other atmospheric conditions. Temperature responses were measured by repeating CO_2 response curves at 15, 20, 25, 30, 35 and 40 ºC, using the same protocol described above but with the expanded temperature control kit (Li-6400-88, Li-Cor) added to the gas exchange system. The temperature response data are shown in Figure 2. Temperature response functions were as follows:

(15) $$V_m\left(T_{leaf,K}\right) = V_{m25} \cdot \exp\left(a_v\left(T_{ref}^{-1} - T_{leaf,K}^{-1}\right)\right),$$

(16) $$J_m\left(T_{leaf,K}\right) = J_{m25} \cdot \exp\left(a_j\left(T_{ref}^{-1} - T_{leaf,K}^{-1}\right)\right) \cdot \left(\frac{1+\exp\left(b_j\right)}{1+\exp\left(b_j + c_j\left(T_{ref}^{-1} - T_{leaf,K}^{-1}\right)\right)}\right), \text{ and}$$

(17) $$g_m\left(T_{leaf}\right) = g_{m25} \cdot \exp\left(-d\left(\ln\left(T_{leaf}/T_{opt}\right)\right)^2\right),$$

where T_{ref} = 298.15 K, $T_{leaf,K}$ is leaf temperature in Kelvins, and a_v, a_j, b_j, c_j, d and T_{opt} are empirical parameters: a_v = 7350.45 K, a_j = 6710.22 K, b_j = -2.15188 (unitless), c_j = 13807.8 K, d = 0.71027 (unitless) and T_{opt} = 36.75 °C. Other parameters were taken from literature: 25°C values and temperature responses for Rubisco kinetic parameters (K_c and K_o) and the photorespiratory CO_2 compensation point (Γ_*) were taken from Bernacchi *et al.* (2003). Non-photorespiratory CO_2 release in the light at 25°C (R_{d25}) was estimated from photosynthetic

response curves as $0.0089 \cdot V_{m25}$ according de Pury and Farquhar (1997), and the temperature response of R_d was taken from Bernacchi *et al.* (2003).

Measuring leaf gas exchange in situ

At each of five times on a given day (approximately 0915, 1100, 1345, 1600 and 1830, CEDT), we used an open flow gas exchange system (Li-6400, Li-Cor) equipped with a clear chamber (Li-6400-08) to obtain a 30-second average measurement of stomatal conductance and incident PPFD on each of the leaves for which we had previously estimated photosynthetic parameters as described above. Prior to each measurement, we observed the leaf's orientation, and oriented the chamber such that the PPFD sensor surface was parallel to the original plane of the leaf; this ensured that the PPFD thus measured was very similar to the PPFD actually experienced by the leaf prior to measuring g_s. c_a was set at 400 μmol mol^{-1} and chamber air temperature and humidity were set to match ambient. Of the 280 expected measurements (5 times x 14 positions x 4 individuals), 10 were lost due to clerical errors, leaving 270 measurements.

Computing ∂A/∂E

We calculated $\partial A/\partial E$ numerically, as follows. We computed A and E from the gas exchange model outlined above, added a very small increment ($1.0 \cdot 10^{-6}$ mol m^{-2} s^{-1}) to stomatal conductance and estimated $\partial A/\partial E$ as the ratio of the resulting increases in A and E. This ensured that changes in leaf temperature (T_{leaf}) resulting from the simulated increment in g_s, and the effects of those temperature changes on both A and E, would be calculated accurately (analytical description of the effects of changing T_{leaf} would be overly complex and prone to error, due to the many photosynthetic parameters affected by T_{leaf}). We verified that this numerical approach did

not suffer from discretisation error by computing $\partial A/\partial E$ both numerically and analytically (using expressions given by Buckley *et al.*, 2002) while holding leaf temperature constant; the two resulting values of $\partial A/\partial E$ were indistinguishable (not shown).

Computing optimal stomatal conductance

For each point in time at each crown position, we computed optimal stomatal conductance as follows. First, we generated the theoretical A vs E relationship for that point by varying g_s from $2.0 \cdot 10^{-4}$ to 2.0 mol m^{-2} s^{-1} in 10,000 steps. We then classified each point into one of three categories based on the nature of the resulting A vs E relationship. In Category I, $\partial A/\partial E$ declines monotonically as g_s increases (i.e., $\partial^2 A/\partial E^2 < 0$). In Category II, $\partial A/\partial E$ increases at low g_s, reaches a maximum and then decreases at higher g_s (i.e., $\partial^2 A/\partial E^2 > 0$ at low g_s and $\partial^2 A/\partial E^2 < 0$ at high g_s). In Category III, $\partial A/\partial E$ is below its crown-wide target value (μ, discussed below) for all positive g_s (typically because PPFD is quite low or Δw is quite high). Examples of relationships between g_s and $\partial A/\partial E$ for five randomly chosen instances of each Category are shown in Figure 3A.

Identification of optimal g_s (g_{so}) differs for each of these categories. For Category III, g_{so} is zero. The category most clearly relevant to the original Cowan-Farquhar theory is Category I; in this case, g_{so} is the value of g_s for which $\partial A/\partial E$ equals a target value, μ, that is invariant among leaves in the crown and over time (the choice of μ is discussed below). For Category II, there exists a realistic positive g_s that maximises instantaneous water use efficiency, WUE = A/E; this occurs when $A/E = \partial A/\partial E$ (Buckley *et al.*, 1999) (Figure 3B). WUE is always greater at that value of g_s than for any other value, including any value (or values) for which $\partial A/\partial E = \mu$. However,

317 although this value of g_s would maximise WUE for a Category II leaf considered by itself, it is
318 not optimal for the crown as a whole. For example, imagine a Category I leaf and a Category II
319 leaf both initially at $\partial A/\partial E = \mu$ (Figure 4A). Consider the effect of reducing E and g_s in the
320 Category II leaf in order to bring it to the point of maximum WUE, where $\partial A/\partial E = A/E$, and
321 redistributing the water thus saved to the Category I leaf (Figure 4B). The total change in
322 assimilation rate resulting from this redistribution is
323
324 (18) $$\delta A_{total} = \int \left(\frac{\partial A}{\partial E}_{I} - \frac{\partial A}{\partial E}_{II} \right) dE ,$$
325
326 where the subscripts I and II refer to variables in the Category I and II leaves, respectively.
327 Because $\partial A/\partial E$ is greater in the Category II leaf than in the Category I leaf across the range of g_s
328 spanning this redistribution (Figure 4B), the integrand in Eqn 18 is negative, so the net change in
329 assimilation rate for both leaves combined is also negative (Figure 4C). Thus, the optimal
330 solution when some leaves are in Category II is to increase transpiration in those leaves at the
331 expense of other leaves until $\partial A/\partial E$ is invariant among all transpiring leaves.
332
333 We identified the optimal g_s in both Category I and II leaves by searching the array of 10,000 g_s
334 and $\partial A/\partial E$ values in reverse (i.e., beginning at high g_s and proceeding towards low g_s), finding
335 the first point where $\partial A/\partial E > \mu$, and identifying optimal g_s as the average of the two values
336 spanning the change in sign of $\partial A/\partial E$. In 21 instances of Category II points, (7.8% of all points),
337 maximum WUE occurred at $g_s > 2.0$ mol m^{-2} s^{-1}; in these cases, we set g_{so} to 2.0 mol m^{-2} s^{-1} on
338 the grounds that values greater than that are not physiologically realistic. We compared the

resulting distributions of water loss with alternative simulations in which g_{so} was either capped at 1.0 mol m^{-2} s^{-1} or allowed to take on arbitrarily high values, and the results were nearly identical (not shown); this is because boundary layer conductance (g_{bw}) was typically quite low in those instances, so that E was relatively insensitive to changes in g_s.

We identified the target value for $\partial A/\partial E$ (μ) separately for each individual by adjusting an initial estimate of μ repeatedly (re-optimising g_s for all measurement points at each value of μ) until the whole-crown diurnal total water loss computed for the optimal pattern of g_s was as close as possible to the total water loss computed for the measured pattern of g_s. Because changes in μ sometimes caused one or more measurement points to change categories, the relationship between μ and total crown water loss was not smooth, so it was not possible to achieve arbitrarily precise agreement in crown total water use between optimal and measured g_s distributions. However, the two values agreed to within 1.53% in all cases, and to within 0.21% when summed over all four crowns. To account for the effect of small remaining differences between measured and optimised crown water loss on comparisons of total carbon gain, we applied an approximate correction to total carbon gain: (Corrected optimal crown A) = (Computed optimal crown A) × (Measured crown E)/(Computed optimal crown E).

Numerical methods

All of the calculations described above were implemented in Microsoft Excel, in some cases using algorithms coded in VBA and in other cases using worksheet formulas. The Excel file containing the code is available from the authors upon request.

Statistical tests of the optimisation hypothesis

We chose to compare transpiration rate, rather than stomatal conductance itself, between optimal and measured patterns, for two reasons. First, mean optimal g_s was many times greater than mean measured g_s in some leaves, due to low boundary layer conductance (when g_{bw} is low, E is nearly insensitive to g_s at high g_s), and this made direct comparisons between measured and optimal patterns of g_s somewhat uninformative. Second, because optimisation theory is concerned with optimal allocation of finite resources, we felt it was more informative to compare distributions of the resource itself (water loss, E) rather than the biological parameter (g_s) that controls how that resource is distributed.

Residuals of E (optimal minus measured E) were distributed highly non-normally (as were the residuals of g_s), and normality could not be adequately improved by any transformation, so we used non-parametric tests (Kruskal-Wallis rank sum test) to assess the probability that observed systematic differences in residual E among crown positions, among times of day, and among times of day at each crown position, were due to chance alone. We also assessed variation in mesophyll conductance (g_{m25}) with crown position using the Kruskal-Wallis test. Variations in photosynthetic capacity (V_{m25} and J_{m25}) were distributed normally, and were assessed by traditional analysis of variance in linear models. All analyses were performed in base R (R Core Team, 2013).

Results

Photosynthetic capacity and irradiance

Photosynthetic capacity estimated from CO_2 response curves (V_{m25} and J_{m25}) differed significantly among crown positions ($p < 0.0001$ for both variables) (Fig 5A,B). Mesophyll conductance (g_{m25}, Fig 5C) also differed among positions ($p = 0.013$). Each of these variables was generally greater in the upper crown (positions 4-7; Fig 1). For comparison, mean PPFD measured *in situ* on the day of diurnal measurements (22 Aug 2012) was greatest at the top of the crown and decreased down the sides of the crown, and PPFD was very low at the three lower interior crown positions (12-14) (Fig 5D).

Atmospheric conditions and associated leaf variables

Atmospheric conditions on 22 Aug 2012 were warm, calm and dry: air temperature ranged from 28.7 to 35.1°C, ambient humidity ranged from 12.0 to 15.5 mmol mol^{-1} (16.5 to 25.4% relative humidity) and 1-hour mean wind speed ranged from 0.5 to 1.1 m s^{-1} (Fig 6). Based on energy balance calculations, crown average leaf temperature (Fig 6B) ranged from 28.7 to 37.4°C, evaporative demand (Δw, Fig 6D) ranged from 27.5 to 59.9 mmol mol^{-1} and boundary layer conductance (g_{bw}, Fig 6F) ranged from 0.19 to 0.28 mol m^{-2} s^{-1}, and each of these variables peaked in early afternoon (1345). Stomatal conductance and water use were moderate despite these conditions, with crown average g_s ranging from a minimum of 0.06 mol m^{-2} s^{-1} (at 1830) to a maximum of 0.13 (at 1100), and transpiration rate reaching a maximum of 4.4 mmol m^{-2} s^{-1} (at 13:45) (Fig 7).

Categorisation of A vs E curves for each point

For each of 270 *in situ* measurement points, we calculated theoretical instantaneous relationships between A and E as described in *Materials and Methods*. Of these 270 points, 49.3% (133/270) were in Category I, for which $\partial A/\partial E$ declines monotonically with increasing g_s. Due to the combination of high irradiance and evaporative demand and low boundary layer conductance, we observed positive curvature in the A vs E relationship ($\partial^2 A/\partial E^2 > 0$) in 39.6% (107/270) of A vs E curves. These points fall into Category II, in which $\partial A/\partial E$ increases at low g_s and decreases at high g_s. Another 11.1% (30/270) were in Category III (optimal g_s was zero because $\partial A/\partial E$ was below the target value, μ, for all positive g_s).

Optimal vs observed gas exchange patterns

The optimal values of g_s were generally quite high, yet this had a smaller effect on total conductance (g_{tw}) and hence transpiration rate (E) than one might expect, due to the low boundary layer conductances. As a consequence, mean g_s predicted by optimisation greatly overestimated measured g_s in many cases, even though total crown water use was identical between the optimal and observed patterns of g_s. This is shown in panels A, C and E of Figure 8, which present measured and predicted g_s in three ways: without any grouping (Fig 8A), grouped by position and averaged over time (Fig 8C), or grouped by time and averaged among positions (Fig 8E).

Because the low boundary layer conductances led to such skewed differences between observed and optimal g_s, comparisons between observed and optimal transpiration rate (E) are more informative, and are presented in panels B, D and F of Figure 8. Optimal E was generally

427 greater than measured *E* in cases where measured *E* itself was higher than the crown average
428 (Figs 8B,D). This pattern largely reflected a reallocation of water loss from the interior crown
429 (positions 11-14) to the upper and east-facing exterior crown (positions 1-6), as illustrated in Fig
430 9A. Residuals of *E* (optimal minus measured *E*) differed significantly among positions ($p <$
431 0.0001). Optimal *E* was also lower than measured *E* in the middle of the day, and higher in the
432 late afternoon (Fig 10A) ($p < 0.05$). Additionally, the variation over time in residuals of *E*
433 differed among crown positions (Fig 11) (these changes were significant for positions 1, 2, 4, 6,
434 8 and 10; $p < 0.05$). The clearest pattern in this regard was for optimal *E* to be greater than
435 measured *E* in the first half of the day on the eastern crown and in the second half of the day on
436 the western crown (Figs 11A,C). Thus, the spatial pattern of differences between optimal and
437 measured *E* among exterior crown positions shown in Fig 9 partly reflects a time-by-position
438 interaction.
439
440 *Effects of gas exchange distributions on total carbon gain*
441 To assess how whole plant carbon/water balance would be impacted by these differences
442 between measured and optimal patterns of water use, we computed total diurnal carbon gain for
443 each crown in three ways: using either the measured or optimal spatio-temporal distributions of
444 g_s or using a constant value of g_s, while controlling for total crown water loss in each case. We
445 found that a constant g_s yielded 71.7 ± 0.6% of the total carbon gain achieved by the optimal g_s
446 distribution, whereas the observed g_s distribution achieved 81.8 ± 0.3% of the optimum (Fig 12).
447

448 *Effects of aerodynamic coupling (boundary layer conductance)*

449 Because boundary layer conductance impacts the validity of the assumption that $\partial^2 A/\partial E^2 < 0$,
450 which underlies optimisation theory, we repeated all calculations under an alternative scenario in
451 which g_{bw} was imagined to be extremely large (which we simulated by setting wind speed to
452 $3 \cdot 10^8$ m s^{-1}). The purpose of comparing the original results to this alternative scenario was to
453 assess the sensitivity of inferred optima to assumptions about aerodynamic coupling between
454 leaves and the air. Some conclusions were qualitatively similar between the "decoupled" and
455 "coupled" scenarios: for example, in both scenarios, the optimal pattern shifted water use from
456 the interior crown to the upper exterior crown (cf. Figs 9A,B), and from early in the day to later
457 in the day. However, some conclusions differed as well. For example, the optimal pattern
458 shifted water use away from positions 3 & 4 on the east face (cf. Figs 9A,B). The magnitude of
459 redistribution of water loss required to achieve the optimum was also greater at many positions
460 in the coupled scenario than in the decoupled scenario (e.g., position 6; cf. Figs 9A,B), although
461 the difference in total carbon gain between the observed g_s distribution and the theoretical
462 optimum was smaller in the coupled scenario (11.6% vs. 18.2%) (Fig 12)
463
464

Discussion

Our objective was to test two aspects of stomatal optimisation theory that have largely been ignored by previous studies. Most work has focused on the prediction that stomata should keep the marginal carbon product of water, $\partial A/\partial E$, invariant over time. However, the theory also predicts that stomata must hold $\partial A/\partial E$ invariant in space (i.e., among leaves in distinct environments within the same individual crown) and it assumes that water loss earns diminishing returns in terms of carbon gain (i.e., the curvature of A vs E is negative: $\partial^2 A/\partial E^2 < 0$) (Cowan & Farquhar, 1977), yet these aspects of the theory remain largely untested. Our results suggest that neither the spatial aspect of the theory nor its assumption of positive curvature hold in grapevine canopies under the hot, dry, sunny and calm conditions typical of Mediterranean summer at our study site. We found that the measured spatial pattern of water use differed systematically from the optimal pattern, with some regions of the crown using more water than the optimum and other regions using less. We also found positive curvature in A vs E for 40% of leaf measurements, largely due to low boundary layer conductance. In addition, we found that if we had simply assumed negligible boundary layer resistance, as many applications of the theory have assumed, then the resulting predictions would have diverged substantially from the true optima, thereby altering some conclusions about the relationship between observed and optimal patterns.

Positive curvature in A vs E and its implications

Water loss typically brings diminishing returns of carbon gain, because stomatal opening tends to reduce the gradient for leaf CO_2 uptake more than that for H_2O loss. As g_s increases, intercellular CO_2 increases, which decreases the CO_2 gradient. Although a related effect occurs

488 with transpiration – that is, increased E can decrease the evaporative gradient (Δw) by increasing
489 ambient humidity – this effect is generally smaller than the CO_2 effect because the volume of air
490 even in a dense canopy is vastly larger than the volume of the intercellular air spaces (Cowan,
491 1977, Buckley *et al.*, 1999). In this case, there is no instantaneous optimum for the tradeoff
492 between carbon gain and water loss: carbon gain per unit of water loss (instantaneous water use
493 efficiency, WUE = A/E) is greatest in the limit of zero g_s, which is a trivial solution. (This is
494 what led Cowan and Farquhar (1977) to ask what pattern of g_s maximises total carbon gain for a
495 given total water loss, which leads to the invariant-$\partial A/\partial E$ solution.) However, increased g_s can
496 strongly reduce Δw when boundary layer conductance (g_{bw}) is low. This is because low g_{bw}
497 weakens convective heat transfer, increasing the scope of evaporative cooling to reduce leaf
498 temperature and therefore Δw (Jones, 1992). The resulting changes in Δw can lead to positive
499 curvature in A vs E (Cowan, 1977, Buckley *et al.*, 1999). In such conditions, there is an
500 instantaneous optimum for leaf-scale WUE, which occurs when $\partial A/\partial E = A/E$ (the point at which
501 the tangent line to the A vs E curve goes through the origin) (Buckley *et al.*, 1999). As a result, it
502 is initially unclear whether the invariant-$\partial A/\partial E$ solution still applies in such conditions.
503
504 Buckley *et al.* (1999) suggested that if curvature is positive but a leaf cannot maintain E high
505 enough to reach the maximum A/E, then the leaf should close some stomata entirely and open
506 others more widely to achieve the optimum in the latter areas; i.e., spatially heterogeneous g_s is
507 beneficial in this case. A related argument can be made at the crown level. If some leaves have
508 negative curvature and others have positive curvature, then water loss should be reallocated from
509 the former to the latter to allow the latter to maximise WUE. This will reduce E in the negative-
510 curvature leaves, thereby increasing $\partial A/\partial E$ and WUE in those leaves as well and ensuring that

511 the reallocation improves WUE throughout the crown. Furthermore, whole-crown WUE is
512 maximised by increasing g_s even further in leaves with positive curvature – i.e., beyond the point
513 at which WUE is maximised for those individual leaves – as explained in the text surrounding
514 Equation 18 and illustrated in Figure 4.
515
516 The Cowan and Farquhar (1977) solution therefore applies even if positive curvature occurs,
517 provided curvature eventually becomes negative at higher g_s. There are two exceptions to this
518 solution. First, stomata should simply open as far as possible in leaves in which $\partial A/\partial E$ is always
519 greater than the crown-wide target value (μ). This scenario applied in 7.8% of measured leaves
520 in the present study. In these cases, boundary layer conductance was very low, so that changes
521 in g_s had very little effect on $\partial A/\partial E$ at high g_s. Second, stomata should simply close in leaves for
522 which the crown-wide target value of $\partial A/\partial E$ (μ) cannot be reached for any g_s ("Category III"
523 leaves in our terminology; Fig 3A); this scenario applied in 11.1% of leaves in this study.
524
525 The implications of positive curvature will depend on how often, in nature, boundary layer
526 conductance is low enough to allow positive curvature to occur. Wind speed above the canopy
527 ranged from 0.5 – 1.1 m s^{-1} in our study, and positive curvature occurred across this range. This
528 range is low but not particularly unusual for our site: mean daytime summer wind speed was
529 0.69 – 0.77 m s^{-1} over 2010-12 (Fig 6e). Another study on grapevine (Daudet *et al.*, 1998) found
530 wind speed was below 1.0 m s^{-1} for 13% of a typical day, and Jones et al. (2002) found wind
531 speed rarely exceeded 1.3 m s^{-1} during two of four days in a field study on grapevine. Similar
532 ranges have been reported in other species (e.g., 1-2 m/s, cotton, Grantz & Vaughn, 1999). Wind
533 speed is much lower inside the crown because of wind attenuation by the canopy itself (e.g.,

534 Oliver, 1971, Daudet *et al.*, 1999, Grantz & Vaughn, 1999). However, this was not a dominant
535 factor in causing positive curvature in the present study, as the occurrence of positive curvature
536 actually decreased with depth in the canopy (Figure 13). We conclude that the occurrence of
537 positive curvature in A vs E may not be as rare as previously thought, and that the matter requires
538 further experimental study.
539
540 *Why is the spatial distribution of water loss sub-optimal?*
541 We found that the observed distribution of water loss among leaves did not match the optimal
542 pattern, that the residuals were systematically related to crown position, and that these deviations
543 reduced crown carbon gain by 18% compared to the optimum. It is helpful here to reiterate the
544 rationale for this definition of "optimal": total carbon gain will be greatest for a given total water
545 loss if $\partial A/\partial E$ is invariant (provided $\partial^2 A/\partial E^2 > 0$). That statement is independent of spatial or
546 temporal scale, and is a generic mathematical result from the calculus of variations (Cowan &
547 Farquhar, 1977). It says that among all possible spatiotemporal distributions of g_s that give the
548 same total crown water loss, carbon gain is greatest for the distribution in which $\partial A/\partial E$ is
549 invariant. A separate question is, at what scale is it biologically meaningful to view total water
550 loss as invariant (Cowan, 1982, Cowan, 1986, Mäkelä *et al.*, 1996, Buckley & Schymanski,
551 2013)? In the next section ("*Is the optimisation problem correctly posed?*"), we discuss the
552 possibility that it is not biologically appropriate to view total crown water loss as invariant,
553 regardless of time scale. In this section we discuss other possible explanations for the observed
554 spatial deviations from optimality. One involves delays in stomatal opening. We found that
555 optimal water loss typically exceeded observed water loss whenever the sun was oriented most
556 directly towards a particular crown position (e.g., Fig 11). It is possible that stomata in these

positions could not respond quickly enough to the peak in PPFD to achieve optimal water loss. This effect would be exacerbated by low g_{bw}, which requires large changes in g_s to achieve a given change in water loss. Vico *et al.* (2011) suggested that delays in stomatal opening and closing in response to changes in PPFD create a quasi-optimal pattern of g_s, arguing that the costs of stomatal regulation itself must be subtracted from leaf net carbon gain in computing the optimum, so that the true optimum includes a finite time constant for stomatal adjustments to PPFD. This is unlikely to explain our results, given that the carbon cost of stomatal movements was on the order of 0.25% of net assimilation rate in the simulations presented by Vico *et al* (2011) – far less than the potential improvement in carbon gain that could have been achieved by optimal stomatal control in our study.

Medlyn et al (2011; 2013) suggested that stomata lack the physiological machinery to detect the shift between carboxylation- and regeneration-limited photosynthesis. Those authors noted that stomatal responses to short-term changes in atmospheric CO_2 were approximately optimal under regeneration- but not carboxylation-limited conditions, so they suggested that stomata were only capable of optimal behaviour under regeneration-limited conditions (i.e., under sub-saturating PPFD). Our results offer qualified support for that idea, as deviations from optimality at a given position tended to be greater when the sun was oriented more directly towards that position, at which time PPFD would likely be saturating.

The spatial distribution of photosynthetic nitrogen may also have contributed to these deviations. The ratio of carboxylation capacity to PPFD was eight times greater in the interior crown (positions 11-14) than on the upper exterior crown (positions 4-7) (Fig 5) – consistent with other

reports that capacity is not proportional to local irradiance, contrary to the predictions of optimisation theory for distribution of photosynthetic nitrogen (Evans, 1993, Hirose & Werger, 1994, Hollinger, 1996, de Pury & Farquhar, 1997, Makino *et al.*, 1997, Bond *et al.*, 1999, Friend, 2001, Frak *et al.*, 2002, Kull, 2002, Lloyd *et al.*, 2010, Buckley *et al.* 2013). It is well established that g_s is highly correlated with photosynthetic capacity (Wong *et al.*, 1979). If this correlation represents a mechanistic constraint on stomatal regulation – i.e., if the mechanisms that stomata have presumably evolved to optimise carbon/water balance include a physiological "response" to photosynthetic capacity or some proxy thereof – then such a response may present a physiological barrier to achieving optimal distributions of water loss in situations where photosynthetic capacity is suboptimally distributed. This highlights the important linkage between the economics of water loss and photosynthetic nitrogen use in plant crowns (Field, 1983, Buckley *et al.*, 2002, Farquhar *et al.*, 2002, Peltoniemi *et al.*, 2012, Buckley *et al.*, 2013, Buckley & Warren, 2013, Palmroth *et al.*, 2013).

Is the optimisation problem correctly posed?

The requirement that $\partial A/\partial E$ be spatially invariant within the crown assumes that water loss can be arbitrarily allocated among leaves and over time within the crown. However, hydraulic constraints may make it impossible for leaves in some crown positions to achieve optimal water loss rates while also maintaining water potential above thresholds for catastrophic loss of hydraulic conductivity. Although this could be remedied by increasing hydraulic conductance to such leaves by re-allocating carbon, such re-allocation may itself be sub-optimal, for two reasons. One is that stem carbon serves other functions, including mechanical support. Another is that hydraulic limitations to water loss may only manifest during brief periods in the growing

603 season, in which case the large carbon investment needed to achieve optimal distribution of
604 water loss may outweigh any resulting gains in crown water use efficiency. Thus, each leaf may
605 in fact require a different target value for $\partial A/\partial E$ to reflect the realities of its water supply
606 constraints. A full exploration of this idea requires more intensive theoretical analysis.
607
608 *Conclusions*
609 We found systematic divergence between observed and optimal spatial patterns of water use, and
610 evidence of widespread positive curvature ($\partial^2 A/\partial E^2 > 0$) in grapevine crowns under hot, dry and
611 calm conditions. Positive curvature resulted from aerodynamic decoupling between the crown
612 and atmosphere. Our results suggest caution is warranted when using optimisation theory to
613 predict g_s at the crown scale, and that further study is required to assess the occurrence of
614 conditions leading to positive curvature. We also suggest it may be necessary to revise
615 optimisation theory to account for variations in hydraulic capacity within a crown.
616
617 **Acknowledgements**
618 This work was funded by the Spanish Ministry of Science and innovation (research projects
619 AGL2008-04525-C02-01, AGL2011-30408-C04-01, and AGL2009-11310/AGR). TNB was
620 supported by the US National Science Foundation (Award #1146514) and by the Grains
621 Research and Development Corporation (GRDC). SM benefited from a FPI grant BES-2009-
622 016906 from the Spanish Ministry of Science and Innovation. The authors thank Dr. Joan
623 Cuxart for meteorological data, Stan Schymanski and Graham Farquhar for helpful
624 conversations, and two anonymous reviewers and the Associate Editor, Dr Danielle Way, for

helpful comments on an earlier draft. We are particularly indebted to a reviewer who noted a critical error in our identification of optimal g_s in Category II leaves.

References

Abramowitz M. & Stegun I.A. (1972) Solutions of quartic equations. In: *Handbook of Mathematical Functions with Formulas, Graphs and Mathematical Tables*, pp. 17-18. Dover, New York.

Ball M.C. & Farquhar G.D. (1984) Photosynthetic and Stomatal Responses of Two Mangrove Species, Aegiceras corniculatum and Avicennia marina, to Long Term Salinity and Humidity Conditions. *Plant Physiology*, **74**, 1-6.

Bernacchi C., Pimentel C. & Long S. (2003) In vivo temperature response functions of parameters required to model RuBP-limited photosynthesis. *Plant, Cell & Environment*, **26**, 1419-1430.

Berninger F., Mäkelä A. & Hari P. (1996) Optimal control of gas exchange during drought: empirical evidence. *Annals of Botany*, **77**, 469-476.

Bond B.J., Farnsworth B.T., Coulombe R.A. & Winner W.E. (1999) Foliage physiology and biochemistry in response to light gradients in conifers with varying shade tolerance. *Oecologia*, **120**, 183-192.

Brenner A.J. & Jarvis P.G. (1995) A heated leaf replica technique for determination of leaf boundary layer conductance in the field. *Agricultural and Forest Meteorology*, **72**, 261-275.

Buckley T.N., Cescatti A. & Farquhar G.D. (2013) What does optimisation theory actually predict about crown profiles of photosynthetic capacity, when models incorporate greater realism? *Plant, Cell & Environment*, **36**, 1547-1563.

Buckley T.N., Farquhar G.D. & Mott K.A. (1999) Carbon-water balance and patchy stomatal conductance. *Oecologia*, **118**, 132-143.

Buckley T.N., Miller J.M. & Farquhar G.D. (2002) The mathematics of linked optimisation for nitrogen and water use in a canopy. *Silva Fennica*, **36**, 639-669.

Buckley T.N. & Mott K.A. (2013) Modeling Stomatal Conductance in Response to Environmental Factors. *Plant, cell & environment*.

Buckley T.N. & Schymanski S.J. (2013) Stomatal optimisation in relation to atmospheric CO2. *New Phytologist*.

Buckley T.N. & Warren C.R. (2013) The role of mesophyll conductance in the economics of nitrogen and water use in photosynthesis. *Photosynthesis Research*, **(doi 10.1007/s11120-013-9825-2)**.

Caemmerer S. & Farquhar G.D. (1981) Some relationships between the biochemistry of photosynthesis and the gas exchange of leaves. *Planta*, **153**, 376-387.

Cowan I. (2002) Fit, fitter, fittest; where does optimisation fit in? *Silva Fennica*, **36**, 745-754.

Cowan I.R. (1977) Stomatal behaviour and environment. *Advances in Botanical Research*, **4**, 117-228.

Cowan I.R. (1982) Water use and optimization of carbon assimilation. In: *Encyclopedia of plant physiology. 12B. Physiological plant ecology* (eds O.L. Lange, C.B. Nobel, C.B. Osmond, & H. Ziegler), pp. 589-630. Springer-Verlag, Berlin.

669 Cowan I.R. (1986) Economics of carbon fixation in higher plants. In: *On the economy of plant*
670 *form and function* (ed T.J. Givnish), pp. 133-170. Cambridge University Press,
671 Cambridge.
672 Cowan I.R. & Farquhar G.D. (1977) Stomatal function in relation to leaf metabolism and
673 environment. *Symposium of the Society for Experimental Biology*, **31**, 471-505.
674 Damour G., Simonneau T., Cochard H. & Urban L. (2010) An overview of models of stomatal
675 conductance at the leaf level. *Plant, Cell & Environment*, **33**, 1419-1438.
676 Daudet F., Le Roux X., Sinoquet H. & Adam B. (1999) Wind speed and leaf boundary layer
677 conductance variation within tree crown: consequences on leaf-to-atmosphere coupling
678 and tree functions. *Agricultural and Forest Meteorology*, **97**, 171-185.
679 Daudet F., Silvestre J., Ferreira M., Valancogne C. & Pradelle F. (1998) Leaf boundary layer
680 conductance in a vineyard in Portugal. *Agricultural and forest meteorology*, **89**, 255-267.
681 de Pury D.G.G. & Farquhar G.D. (1997) Simple scaling of photosynthesis from leaves to
682 canopies without the errors of big-leaf models. *Plant, Cell and Environment*, **20**, 537-
683 557.
684 Ethier G. & Livingston N. (2004) On the need to incorporate sensitivity to CO2 transfer
685 conductance into the Farquhar–von Caemmerer–Berry leaf photosynthesis model. *Plant,*
686 *Cell & Environment*, **27**, 137-153.
687 Evans J.R. (1993) Photosynthetic acclimation and nitrogen partitioning within a lucerne canopy.
688 II. Stability through time and comparison with a theoretical optimum. *Australian Journal*
689 *of Plant Physiology*, **20**, 69-82.
690 Farquhar G.D. (1973) *A study of the responses of stomata to perturbations of environment*, The
691 Australian National University.
692 Farquhar G.D., Buckley T.N. & Miller J.M. (2002) Stomatal control in relation to leaf area and
693 nitrogen content. *Silva Fennica*, **36**, 625-637.
694 Farquhar G.D., Schulze E.D. & Kuppers M. (1980a) Responses to humidity by stomata of
695 Nicotiniana glauca L. and Corylus avellana L. are consistent with the optimization of
696 carbon dioxide uptake with respect to water loss. *Australian Journal of Plant Physiology*,
697 **7**, 315-327.
698 Farquhar G.D., von Caemmerer S. & Berry J.A. (1980b) A biochemical model of photosynthetic
699 CO_2 assimilation in leaves of C_3 species. *Planta*, **149**, 78-90.
700 Field C.B. (1983) Allocating nitrogen for the maximization of carbon gain: leaf age as a control
701 on the allocation program. *Oecologia*, **56**, 341-347.
702 Fites J. & Teskey R. (1988) CO2 and water vapor exchange of Pinus taeda in relation to stomatal
703 behavior: test of an optimization hypothesis. *Canadian Journal of Forest Research*, **18**,
704 150-157.
705 Frak E., Le Roux X., Millard P., Adam B., Dreyer E., Escuit C., Sinoquet H., Vandame M. &
706 Varlet-Grancher C. (2002) Spatial distribution of leaf nitrogen and photosynthetic
707 capacity within the foliage of individual trees: disentangling the effects of local light
708 quality, leaf irradiance, and transpiration. *Journal of Experimental Botany*, **53**, 2207-
709 2216.
710 Friend A.D. (2001) Modelling canopy CO2 fluxes: are 'big-leaf' simplifications justified?
711 *Global Ecology and Biogeography*, **10**, 603-619.
712 Gates D.M., Keegan H.J., Schleter J.C. & Weidner V.R. (1965) Spectral properties of plants.
713 *Applied optics*, **4**, 11-20.

714 Grantz D.A. & Vaughn D.L. (1999) Vertical profiles of boundary layer conductance and wind
715 speed in a cotton canopy measured with heated brass surrogate leaves. *Agricultural and*
716 *Forest Meteorology*, **97**, 187-197.
717 Guehl J.-M. & Aussenac G. (1987) Photosynthesis Decrease and Stomatal Control of Gas
718 Exchange in Abies alba Mill. in Response to Vapor Pressure Difference. *Plant*
719 *Physiology*, **83**, 316-322.
720 Hari P., Mäkelä A., Berninger F. & Pohja T. (1999) Field evidence for the optimality hypothesis
721 of gas exchange in plants. *Australian Journal of Plant Physiology*, **26**, 239-244.
722 Hirose T. & Werger M.J.A. (1994) Photosynthetic capacity and nitrogen partitioning among
723 species in the canopy of a herbaceous plant community. *Oecologia*, **100**, 203-212.
724 Hollinger D.Y. (1996) Optimality and nitrogen allocation in a tree canopy. *Tree Physiology*, **16**,
725 627-634.
726 Jones H.G. (1992) *Plants and microclimate*. (2nd ed.). Cambridge University Press, Cambridge.
727 Jones H.G., Stoll M., Santos T., de Sousa C., Chaves M.M. & Grant O.M. (2002) Use of infrared
728 thermography for monitoring stomatal closure in the field: application to grapevine.
729 *Journal of Experimental Botany*, **53**, 2249-2260.
730 Kull O. (2002) Acclimation of photosynthesis in canopies: models and limitations. *Oecologia*,
731 **133**, 267-279.
732 Küppers M. (1984) Carbon Relations and Competition between Woody Species in a Central
733 European Hedgerow. II. Stomatal Responses, Water Use, and Hydraulic Conductivity in
734 the Root/Leaf Pathway. *Oecologia*, **64**, 344-354.
735 Leuning R. (1988) Leaf temperatures during radiation frost Part II. A steady state theory.
736 *Agricultural and Forest Meteorology*, **42**, 135-155.
737 Leuning R., Kelliher F.M., de Pury D.G.G. & Schulze E.D. (1995) Leaf nitrogen,
738 photosynthesis, conductance and transpiration: scaling from leaves to canopies. *Plant,*
739 *Cell and Environment*, **18**, 1183-1200.
740 Lloyd J., Patino S., Paiva R.Q., Nadrdoto G.B., Quesada C.A., Santos A.J.B., Baker T.R., Brand
741 W.A., Hilke I., Gielmann H., Raessler M., Luizao F.J., Martinelli L.A. & Mercado L.M.
742 (2010) Optimisation of photosynthetic carbon gain and within-canopy gradients of
743 associated foliar traits for Amazon forest trees. *Biogeosciences*, **7**, 1833-1859.
744 Mäkelä A., Berninger F. & Hari P. (1996) Optimal control of gas exchange during drought:
745 theoretical analysis. *Annals of Botany*, **77**, 461-467.
746 Mäkelä A., Givnish T.J., Berninger F., Buckley T.N., Farquhar G.D. & Hari P. (2002)
747 Challenges and opportunities of the optimality approach in plant ecology. *Silva Fennica*,
748 **36**, (in press).
749 Makino A., Sato T., Nakano H. & Mae T. (1997) Leaf photosynthesis, plant growth and nitrogen
750 allocation in rice under difference irradiances. *Planta*, **203**, 390-398.
751 Meinzer F. (1982) The effect of vapor pressure on stomatal control of gas exchange in Douglas
752 fir (Pseudotsuga menziesii) saplings. *Oecologia*, **54**, 236-242.
753 Oliver H. (1971) Wind profiles in and above a forest canopy. *Quarterly Journal of the Royal*
754 *Meteorological Society*, **97**, 548-553.
755 Palmroth S., Katul G.G., Maier C.A., Ward E., Manzoni S. & Vico G. (2013) On the
756 complementary relationship between marginal nitrogen and water-use efficiencies among
757 Pinus taeda leaves grown under ambient and CO2-enriched environments. *Annals of*
758 *botany*, **111**, 467-477.

759 Peltoniemi M.S., Duursma R.A. & Medlyn B.E. (2012) Co-optimal distribution of leaf nitrogen
760 and hydraulic conductance in plant canopies. *Tree Physiology*, **32**, 510-519.
761 Press W.H., Teukolsky S.A., Vetterling W.T. & Flannery B.P. (1992) *Numerical recipes in*
762 *C++: the art of scientific computing*. (2 ed.). Cambridge University Press, Cambridge,
763 UK.
764 Roth-Nebelsick A. (2001) Computer-based analysis of steady-state and transient heat transfer of
765 small-sized leaves by free and mixed convection. *Plant, Cell & Environment*, **24**, 631-
766 640.
767 Sandford A.P. & Jarvis P.G. (1986) Stomatal responses to humidity in selected conifers. *Tree*
768 *Physiology*, **2**, 89-103.
769 Schymanski S.J., Roderick M.L., Sivapalan M., Hutley L.B. & Beringer J. (2008) A canopy-
770 scale test of the optimal water-use hypothesis. *Plant, Cell & Environment*, **31**, 97-111.
771 Team R.C. (2013) R: A language and environment for statistical computing. R Foundation for
772 Statistical Computing, Vienna, Austria.
773 Thomas D.S., Eamus D. & Bell D. (1999) Optimization theory of stomatal behaviour: II.
774 Stomatal responses of several tree species of north Australia to changes in light, soil and
775 atmospheric water content and temperature. *Journal of Experimental Botany*, **50**, 393-
776 400.
777 Vico G., Manzoni S., Palmroth S. & Katul G. (2011) Effects of stomatal delays on the economics
778 of leaf gas exchange under intermittent light regimes. *New Phytologist*, **192**, 640-652.
779 Way D.A., Oren R., Kim H.-S. & Katul G.G. (2011) How well do stomatal conductance models
780 perform on closing plant carbon budgets? A test using seedlings grown under current and
781 elevated air temperatures. *Journal of Geophysical Research: Biogeosciences*, **116**,
782 G04031.
783 Williams W.E. (1983) Optimal water-use efficiency in a California shrub. *Plant, Cell &*
784 *Environment*, **6**, 145-151.
785 Wong S.C., Cowan I.R. & Farquhar G.D. (1979) Stomatal conductance correlates with
786 photosynthetic capacity. *Nature*, **282**, 424-426.
787 World Meteorological Organization (2008) *Guide to Meteorological Instruments and Methods of*
788 *Observation*. WMO, Geneva, Switzerland.
789
790
791

Tables

Table 1. List of variables and parameters referred to in this study, including symbols, units and values where appropriate.

Variable	Symbol	Units	Value
net CO_2 assimilation rate	A	μmol m^{-2} s^{-1}	varies
leaf absorptance to photosynthetic photon flux	α	-	0.92
demand or supply limited value of A	A_d, A_s	μmol m^{-2} s^{-1}	varies
RuBP-carboxylation or regeneration limited value of A_d	A_v, A_j	μmol m^{-2} s^{-1}	varies
ambient CO_2 mole fraction	c_a	μmol mol^{-1}	400
intercellular or chloroplastic CO_2 mole fraction	c_i, c_c	μmol mol^{-1}	varies
molar heat capacity of air	c_p	J mol^{-1} K^{-1}	29.2
curvature of A vs E relationship	$\partial^2 A/\partial E^2$	μmol m^2 s $mmol^{-2}$	varies
saturation vapour pressure deficit of air	D_a	Pa	varies
marginal carbon product of water	$\partial A/\partial E$	μmol $mmol^{-1}$	varies
leaf characteristic dimension	d_{leaf}	m	0.1
effective leaf-air water vapour mole fraction gradient	Δw	mmol mol^{-1}	varies
leaf transpiration rate	E	mmol m^{-2} s^{-1}	varies
leaf emissivity to IR	ε_{leaf}	-	0.95
fraction of absorbed photons that do not contribute to photochemistry	f	-	0.23
absorbed shortwave radiation	Φ	J m^{-2} s^{-1}	varies
fraction of infrared radiation that comes from the sky	f_{ir}	-	varies
psychrometric constant	γ	Pa K^{-1}	66.0
photorespiratory CO_2 compensation point (at 25°C)	Γ_* (Γ_{*25})	μmol mol^{-1}	varies (36.2)
leaf boundary layer conductance to heat, water or CO_2	g_{bh}, g_{bw}, g_{bc}	mol m^{-2} s^{-1}	varies
mesophyll conductance to CO_2	g_m	mol m^{-2} s^{-1}	varies
radiation conductance	g_{Rn}	mol m^{-2} s^{-1}	varies
stomatal conductance to water or CO_2	g_s, g_{sc}	mol m^{-2} s^{-1}	varies
maximum stomatal conductance	g_{smax}	mol m^{-2} s^{-1}	varies
optimal stomatal conductance	g_{so}	mol m^{-2} s^{-1}	varies
total leaf conductance to water or CO_2	g_{tw}, g_{tc}	mol m^{-2} s^{-1}	varies
potential electron transport rate	J	μmol m^{-2} s^{-1}	varies
light-limited (capacity-saturated) value of J	J_i	μmol m^{-2} s^{-1}	varies
capacity-limited (light-saturated) value of J (at 25°C)	J_m (J_{m25})	μmol m^{-2} s^{-1}	varies
Michaelis constant for RuBP carboxylation or oxygenation	K_c, K_o	μmol mol^{-1}	varies
canopy extinction coefficient for diffuse irradiance	k_d	-	0.8
cumulative leaf area index	L	m^2 m^{-2}	varies
target value for $\partial A/\partial E$	μ	μmol $mmol^{-1}$	1.28-1.59
mole fraction of oxygen	O	μmol mol^{-1}	$2.1 \cdot 10^5$
atmospheric pressure	P_{atm}	Pa	$1.0 \cdot 10^5$
photosynthetic photon flux density	PPFD	μmol m^{-2} s^{-1}	varies
curvature parameter for relationship of A_d to A_v and A_j	θ_A	-	0.99
curvature parameter for relationship of J to J_m and J_i	θ_J	-	0.90
non-photorespiratory CO_2 release (at 25°C)	R_d (R_{d25})	μmol m^{-2} s^{-1}	varies
net isothermal radiation	R_n^*	J m^{-2} s^{-1}	varies
Stefan-Boltzmann constant	σ	J m^{-2} s^{-1} K^{-4}	$5.67 \cdot 10^{-8}$
air temperature (in Kelvins)	T_{air} ($T_{air,K}$)	°C (K)	varies
leaf temperature	T_{leaf} ($T_{leaf,K}$)	°C (K)	varies
carboxylation capacity (at 25°C)	V_m (V_{m25})	μmol m^{-2} s^{-1}	varies
wind speed	v_{wind}	m s^{-1}	varies
water vapour mole fraction of intercellular spaces or air	w_i, w_a	mmol mol^{-1}	varies

Table 2. Cumulative leaf area index (L, m^2 m^{-2}) at each of the 14 canopy positions illustrated in Figure 1, used to estimate wind speed at each position (Eqn 14).

position	***L***
1	3.1
2	2.6
3	2.1
4	1.8
5	0
6	0
7	1.5
8	1.8
9	2.4
10	2.7
11	1.6
12	2.1
13	2.6
14	3.3

Figure legends

Figure 1. Diagram illustrating the 14 crown positions at which leaf gas exchange was measured in this study. The diagram represents a cross-section of the grapevine crown, looking southwards along the long axis of a planting row, with east (sunrise) to the left and west (sunset) to the right. Positions 1-10 are on the crown exterior, and positions 11-14 are in the crown interior.

Figure 2. Temperature responses for photosynthetic parameters measured in grapevine for this study (symbols) and response curves fitted to these measurements (lines; Eqns 15-17 in the main text). (b) Electron transport capacity, J_m, (a) carboxylation capacity, V_m, (c) mesophyll conductance to CO_2, g_m.

Figure 3. (A) Relationships between the marginal carbon product of water and g_s for four randomly chosen leaves in each of Category I (for which $\partial^2 A/\partial E^2 < 0$; dashed lines) and Category II (for which $\partial^2 A/\partial E^2 > 0$ at low g_s; solid lines); the thick black horizontal line represents the target value for $\partial A/\partial E$ (μ). (B) The relationships between g_s and $\partial A/\partial E$ (solid line) and instantaneous water use efficiency, A/E (dashed line) for one leaf in Category II, showing that A/E is maximised at a lower g_s (left-hand vertical grey line) than the g_s at which $\partial A/\partial E$ equals the crown-wide target value, μ (right-hand vertical grey line). μ is shown by the horizontal black line. (The curves marked with asterices in A also appear in Figure 4.)

Figure 4. Illustration of the effect of redistributing water loss from a Category II leaf (solid lines) to a Category I leaf (dashed lines) in order to maximise water use efficiency (A/E) in the former. (A, open symbols): initial condition, in which $\partial A/\partial E$ equals the crown-wide target value, μ, for both leaves. (B, closed symbols): condition after redistribution of water loss (δE = 0.552 mmol m^{-2} s^{-1}) from the Category II leaf to the Category I leaf. (C): Relationships between net CO_2 assimilation rate, A, and stomatal conductance, g_s, for both leaves, with symbols representing the initial and final conditions as in A and B. The net change in A resulting from redistribution is negative. (Note that the Category I and II leaves correpond to the curves marked with one and two asterices, respectively, in Figure 3A.)

Figure 5. Gas exchange parameters (A, carboxylation capacity at 25°C, V_{m25}; B, electron transport capacity at 25°C, J_{m25}; C, mesophyll conductance at 25°C, g_{m25}) and incident photosynthetic photon flux density on the day of *in situ* measurements (D, PPFD) at each of 14 crown positions (see diagram in Figure 1). Black bars, exterior crown; grey bars, interior crown. Sample means ± SE.

Figure 6. Environmental conditions measured at a meteorological station adjacent to the study site (A,C,E), and crown averages of associated leaf-level variables calculated from energy balance, based on those environmental conditions (B,D,F). A, air temperature (T_{air}); B, leaf temperature (T_{leaf}); C, ambient water vapour mole fraction (w_a); D, effective leaf-to-air water vapour mole fraction gradient (Δw); E, wind speed (v_{wind}) measured on the day of the study (bars) and averaged over June-August in 2010-2012 (line and symbols); F, boundary layer conductance to water (g_{bw}). For B, D and E, error bars are SEs among four individual crowns.

Figure 7. In situ measurements of stomatal conductance, g_s (A), and values of transpiration rate, E (B) calculated from measured g_s, averaged over 14 crown positions. Error bars are SEs among four individual crowns.

Figure 8. Measured vs optimal stomatal conductance to H_2O g_s (A, C, E) and transpiration rate, E (B, D, F). A, B: averages within each of 70 combinations of crown position and measurement time. C, D: averages over all measurement times within each of 14 crown positions. E, F: averages over all crown positions at each of five measurement times. Error bars are SEs among four individual crowns. Grey lines in B,D,F: one-to-one line. Note the y-axis scales differ in A, C and E.

Figure 9. Residuals of transpiration rate (optimal minus measured E): diurnal means in relation to crown position. A, optimal E computed using boundary layer conductance, g_{bw}, modeled based on measured wind speed. B, optimal E computed assuming negligible boundary layer resistance (infinite g_{bw}). Error bars are SEs among four individual crowns. Note the y-axis scales differ in A and B.

Figure 10. Residuals of transpiration rate (optimal minus measured E): averages over 14 crown positions, shown in relation to time. A, optimal E computed using boundary layer conductance, g_{bw}, modeled based on measured wind speed. B, optimal E computed assuming negligible boundary layer resistance (infinite g_{bw}). Error bars are SEs among four individual crowns. Note the y-axis scales differ in A and B.

Figure 11. Residuals of transpiration rate (optimal minus measured E) over time for each of 14 crown positions: A, positions 1-5 (the eastern side of the crown); B, positions 11-14 (the interior crown); C, positions 6-10 (the western side of the crown). Error bars are SEs among four individual crowns.

Figure 12. Total diurnal carbon gain calculated using either constant g_s, measured g_s or optimised g_s, expressed as a percentage of optimised values. Error bars are SEs among four individual crowns.

Figure 13. Proportion (as percent) of measurement points for which positive curvature in the relationship between assimilation rate and transpiration rate was observed. Position categories are as follows: upper (positions 5 and 6), mid-upper (positions 4 and 7), middle (positions 3 and 8), mid-lower (positions 2 and 9), lower (positions 1 and 10), interior (positions 11-14). Position numbers are shown in Figure 1.

892
893

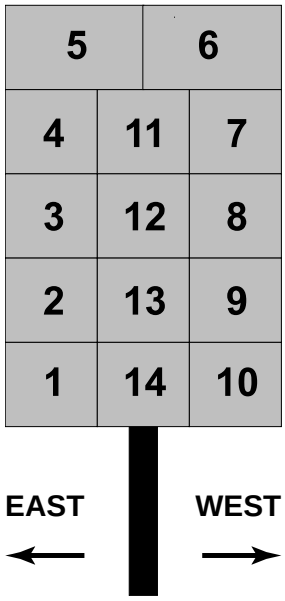

894
895
896 Figure 1
897

898
899

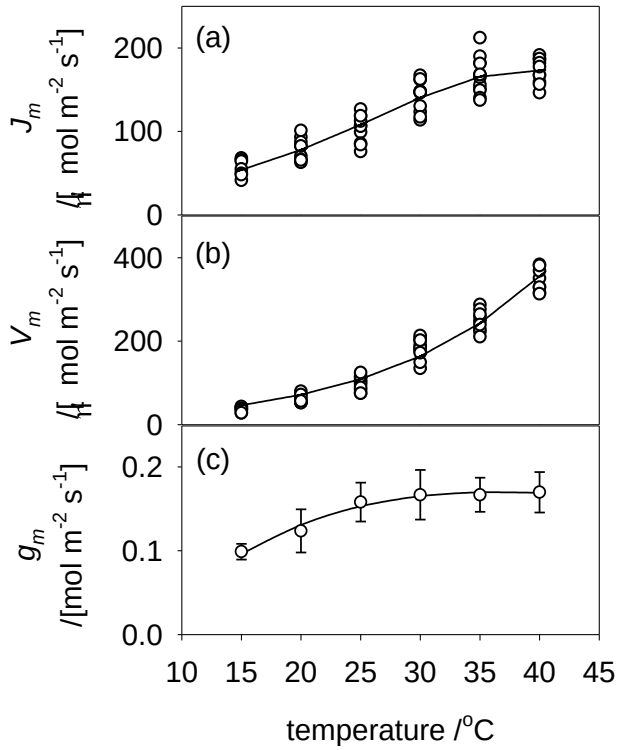

900
901
902
903 Figure 3
904

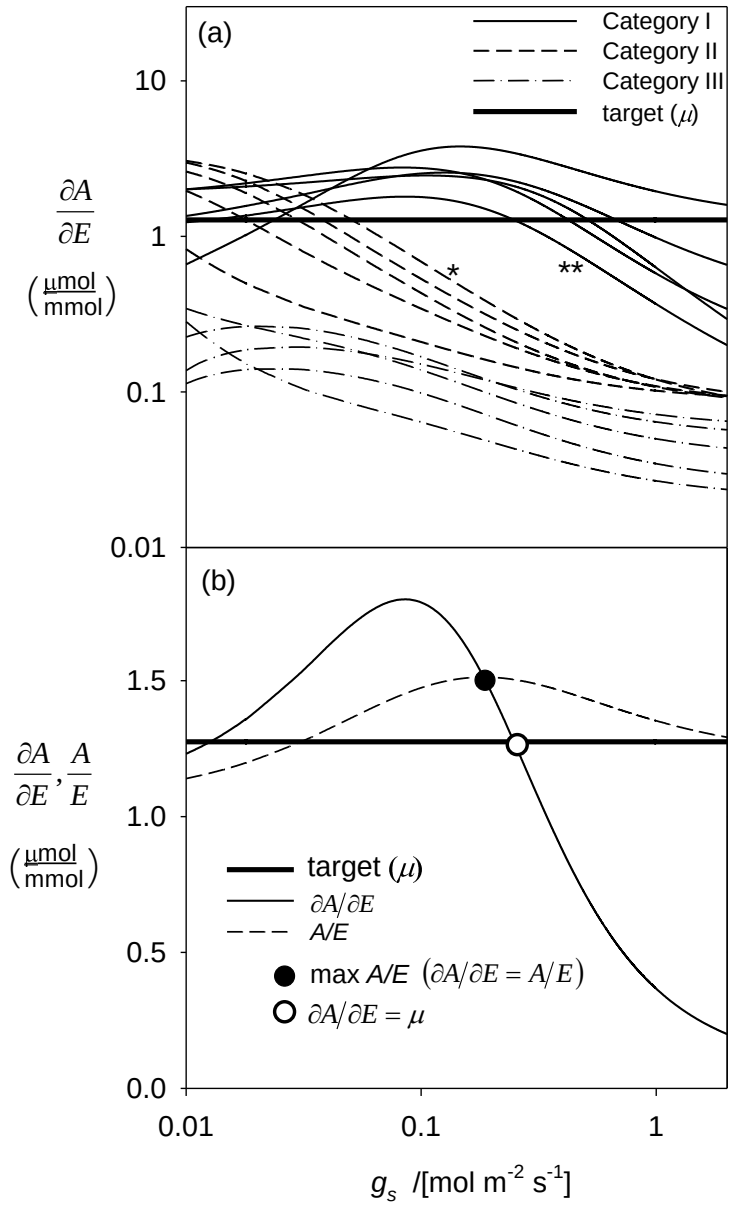
(a)
Category I
Category II
Category III
target (μ)
10
1
0.1
0.01
∂A/∂E
(μmol/mmol)
*
**
(b)
1.5
1.0
0.5
0.0
∂A/∂E, A/E
(μmol/mmol)
target (μ)
∂A/∂E
A/E
max A/E (∂A/∂E = A/E)
∂A/∂E = μ
0.01
0.1
1
g_s /[mol m^-2 s^-1]

Figure 3

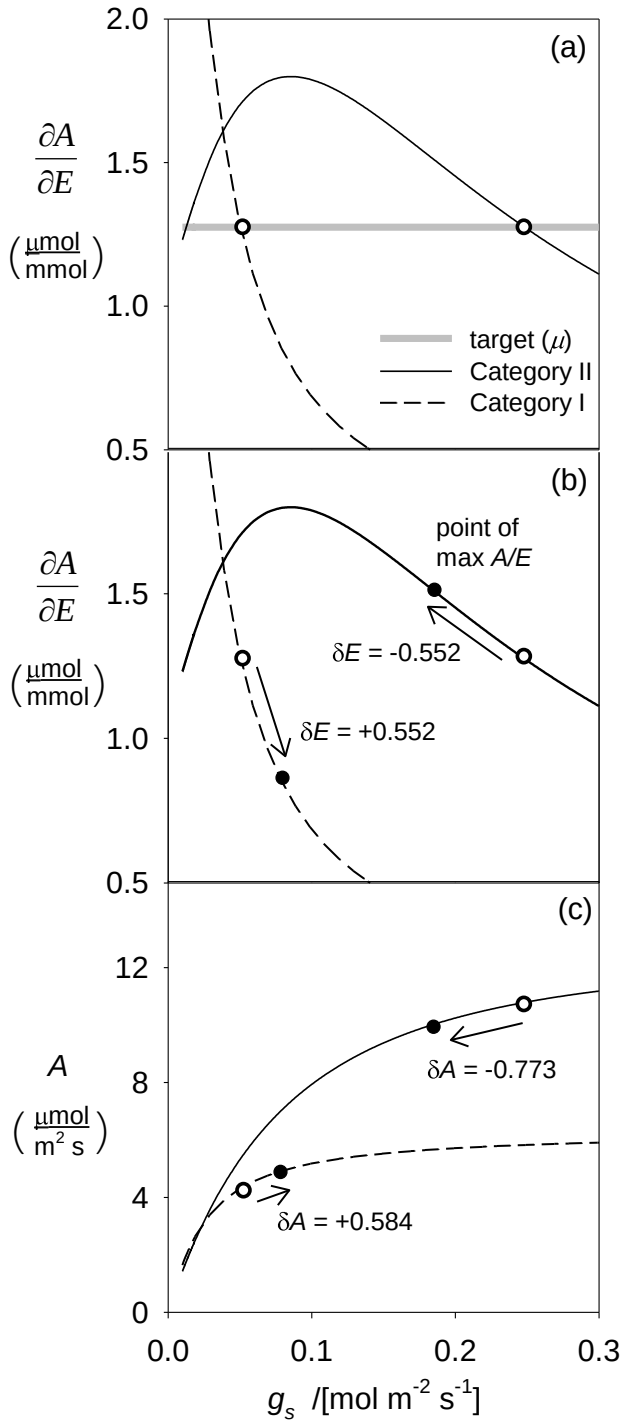
(a)
(b)
(c)
target (μ)
Category II
Category I
point of max A/E
δE = -0.552
δE = +0.552
δA = -0.773
δA = +0.584
∂A/∂E (μmol/mmol)
A (μmol/m² s)
g_s /[mol m⁻² s⁻¹]
2.0
1.5
1.0
0.5
12
8
4
0
0.0
0.1
0.2
0.3

Figure 4

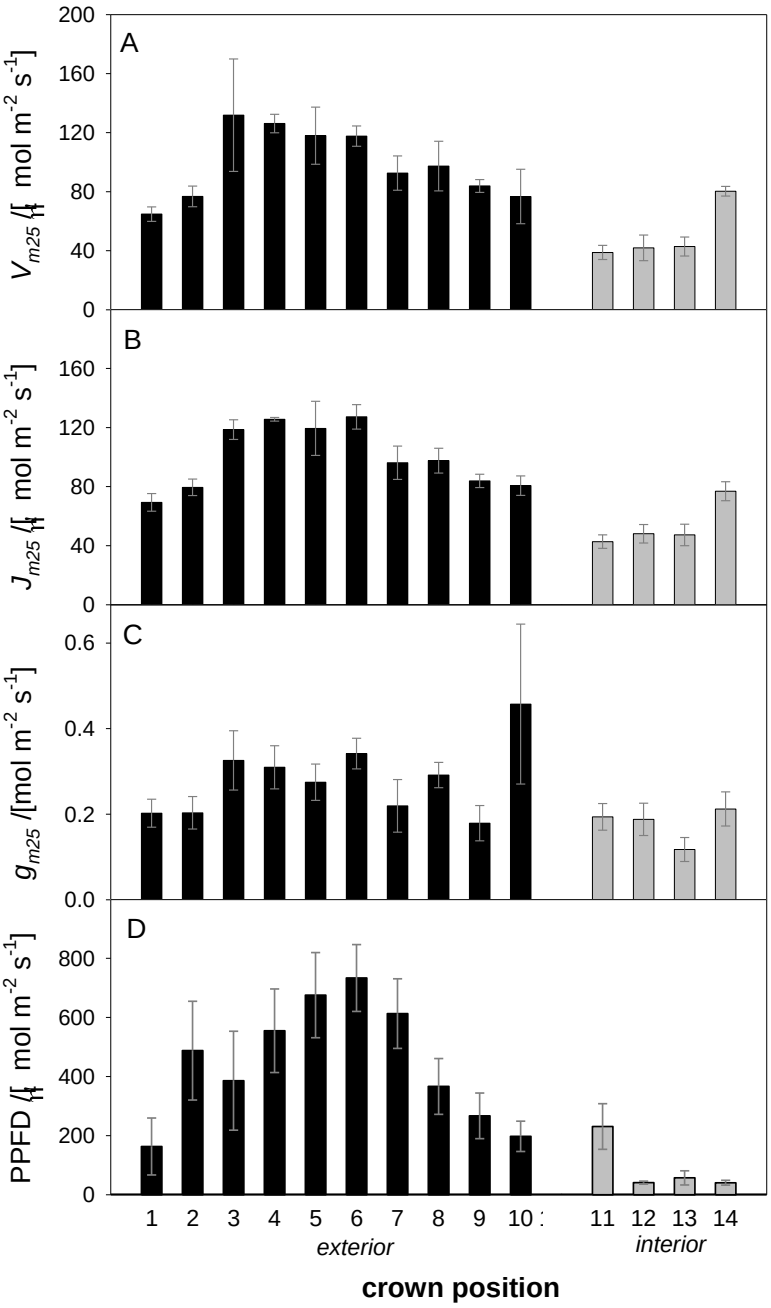
A
B
C
D
200
160
120
80
40
0
0.6
0.4
0.2
0.0
800
600
400
200
1 2 3 4 5 6 7 8 9 10 11 12 13 14
exterior
interior
crown position

Figure 5

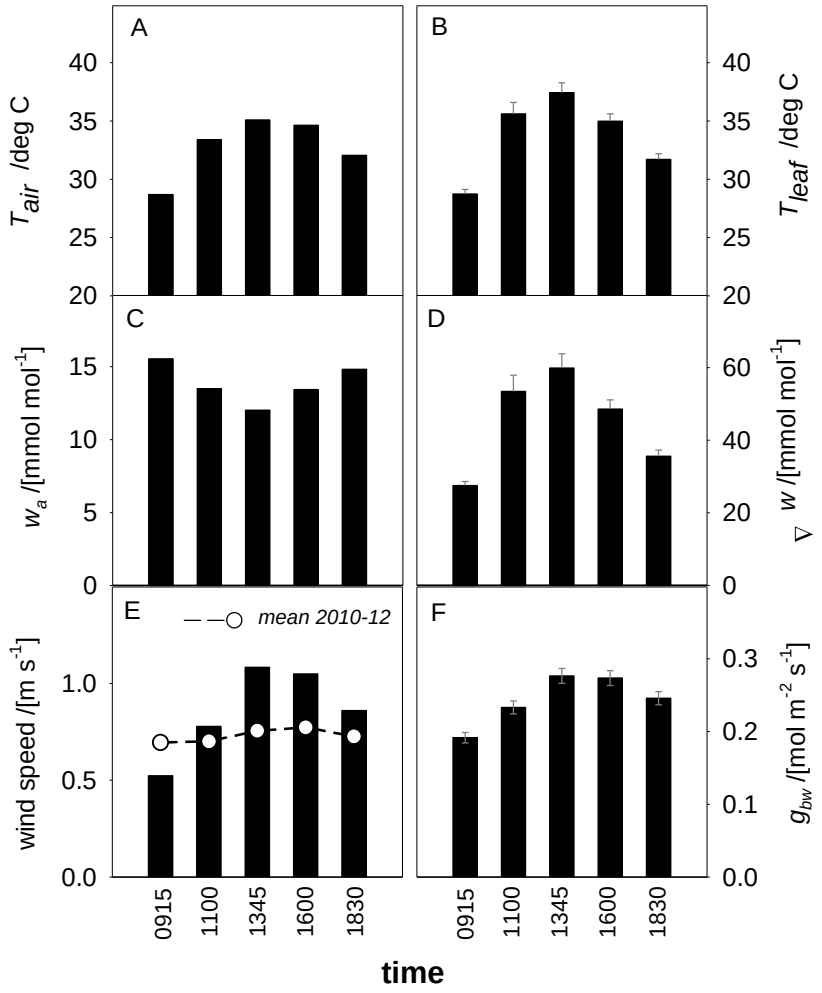
A
B
C
D
E
F
T_{air} /deg C
T_{leaf} /deg C
w_a /[mmol mol^{-1}]
∇w /[mmol mol^{-1}]
wind speed /[m s^{-1}]
g_{bw} /[mol m^{-2} s^{-1}]
mean 2010-12
0915
1100
1345
1600
1830
time

Figure 6

933
934

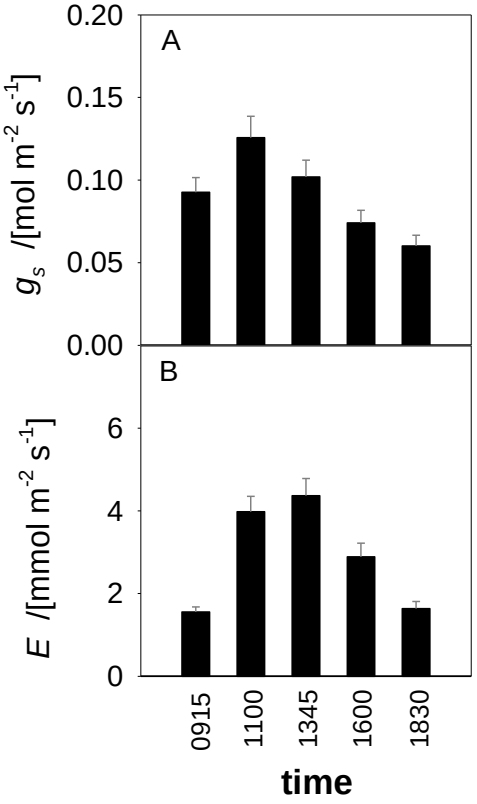

935
936
937
938
939 Figure 7
940

941

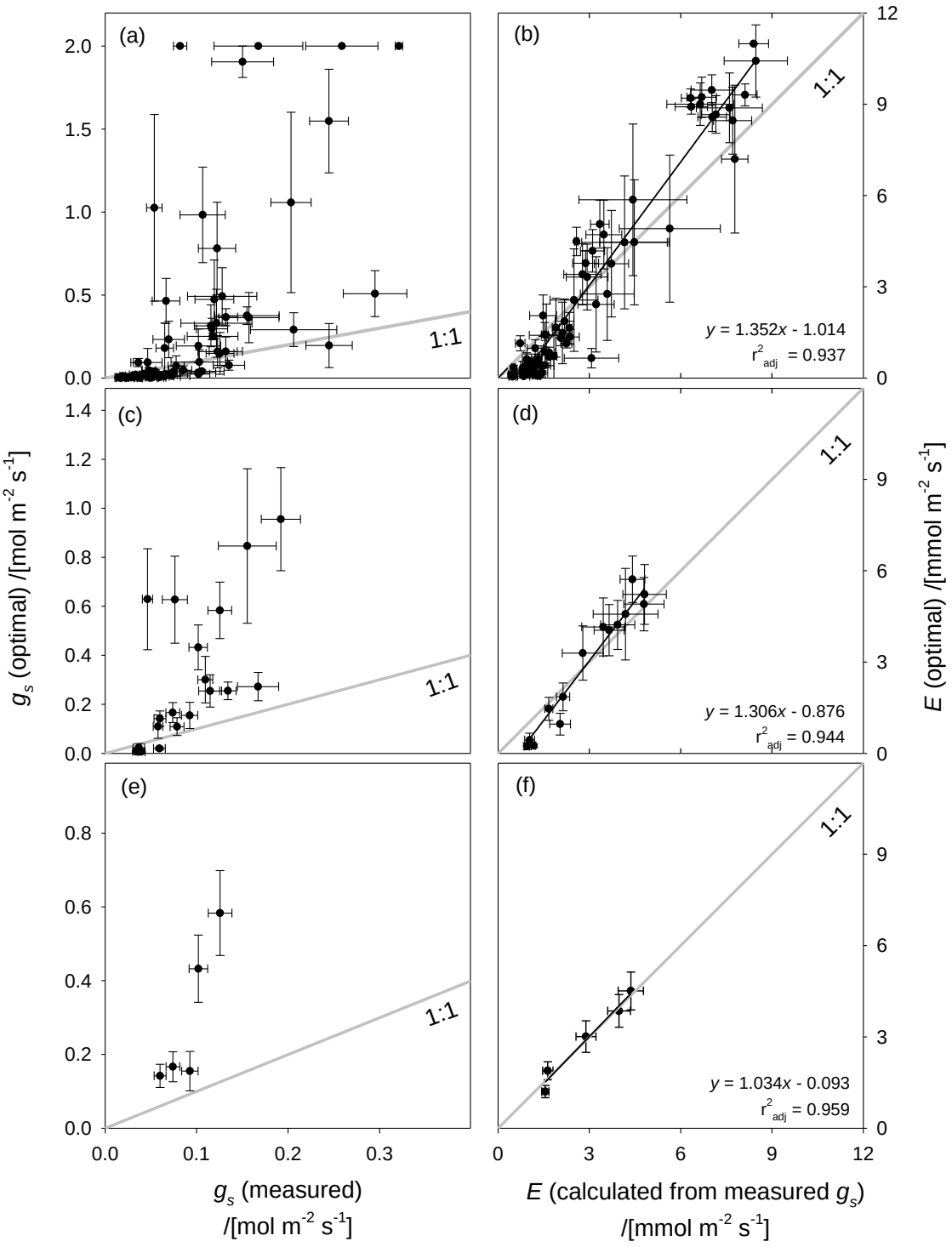

942
943 Figure 8
944
945

946

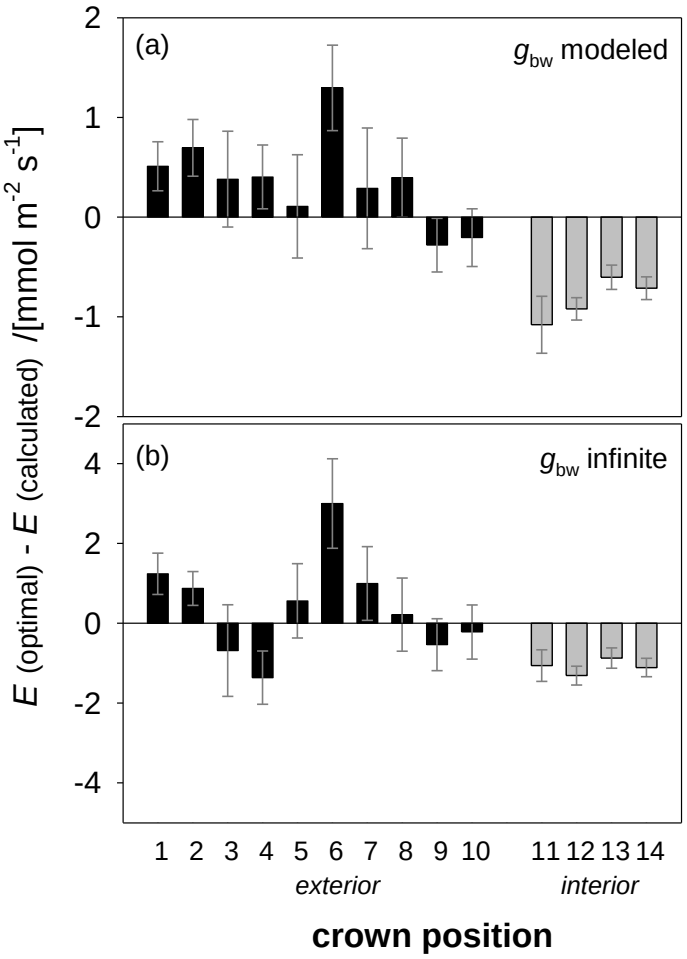

947
948
949
950 Figure 9
951

952

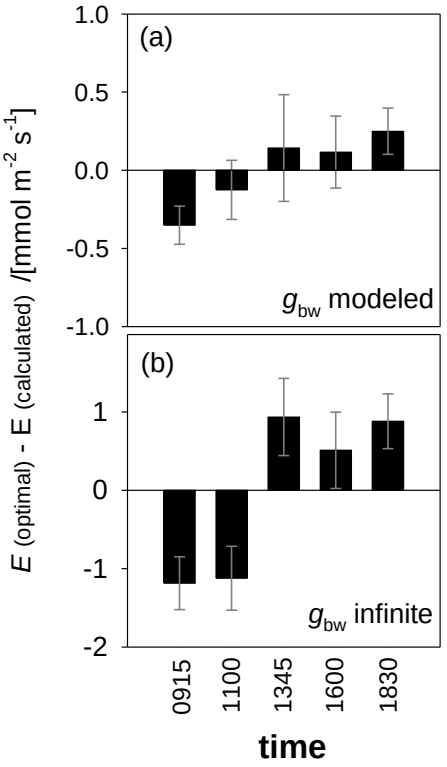

953
954
955
956 Figure 10
957

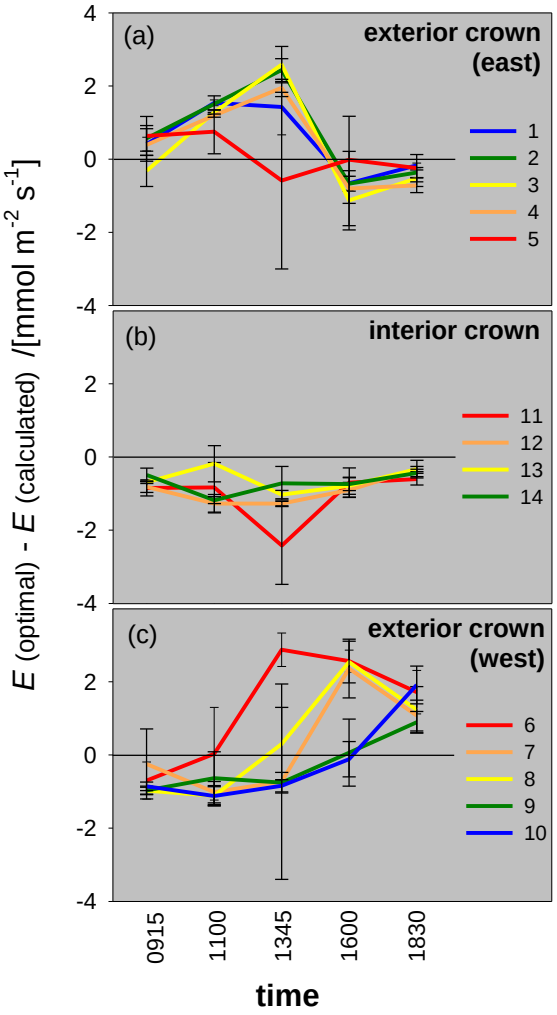
(a)
exterior crown (east)
1
2
3
4
5
(b)
interior crown
11
12
13
14
(c)
exterior crown (west)
6
7
8
9
10
4
2
0
-2
-4
E (optimal) - E (calculated) /[mmol m-2 s-1]
0915
1100
1345
1600
1830
time

Figure 11

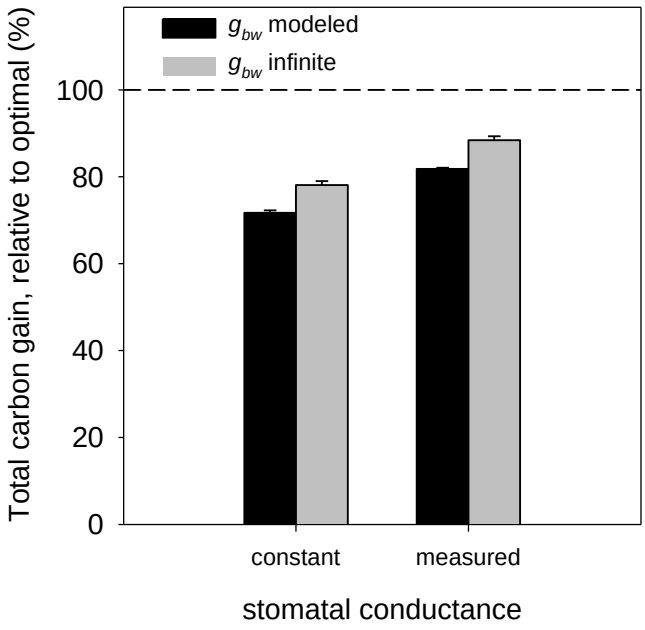
g_{bw} modeled
g_{bw} infinite
Total carbon gain, relative to optimal (%)
100
80
60
40
20
0
constant
measured
stomatal conductance

Figure 12

975
976

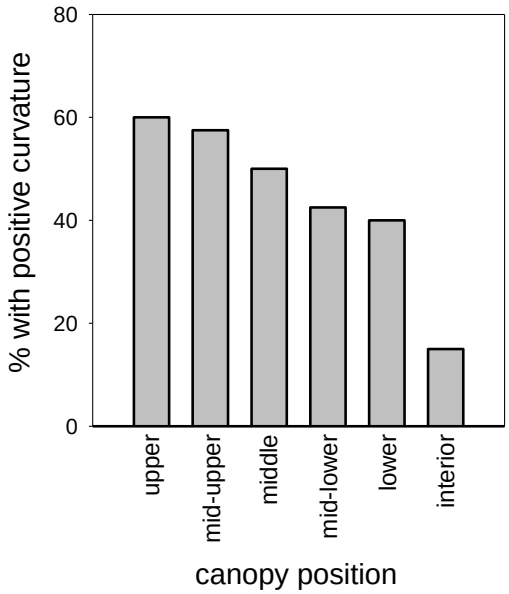

977
978
979
980 Figure 13
981
982
983